NONLINEAR MODEL PREDICTIVE CONTROL OF A LINEAR AXIS BASED ON PNEUMATIC MUSCLES

Harald Aschemann and Dominik Schindele
Chair of Mechatronics, University of Rostock, Justus-von-Liebig-Weg 6, D-18059 Rostock, Germany

Keywords: Mechatronics, predictive control, flatness-based methods, pneumatic muscle.

Abstract: This paper presents a nonlinear optimal control scheme for a mechatronic system that consists of a guided carriage and an antagonistic pair of pneumatic muscles as actuators. Modelling leads to a system of nonlinear differential equations including polynomial approximations of the volume characteristic as well as the force characteristic of the pneumatic muscles. The proposed control has a cascade structure: the nonlinear norm-optimal control of both pneumatic muscle pressures is based on an approximative solution of the corresponding HJB-equation, whereas the outer control loop involves a multivariable NMPC of the carriage position and the mean internal pressure of the pneumatic muscles. To improve the tracking behaviour, the feedback control loops are extended with nonlinear feedforward control based on differential flatness. Remaining model uncertainties as well as nonlinear friction can be counteracted by an observer-based disturbance compensation. Experimental results from an implementation on a test rig show an excellent control performance.

1 INTRODUCTION

Pneumatic muscle actuators are tension actuators consisting of a fiber-reinforced vulcanised rubber tubing with connection flanges at both ends. Due to a special fiber arrangement, the pneumatical muscle contracts with increasing internal pressure. This effect can be used for actuation purposes. Pneumatic muscles offer major advantages in comparison to classical pneumatic cylinders: significantly less weight, no stick-slip effects, insensitivity to dirty working environment, and a larger maximum force. The nonlinear characteristics of the muscle, however, demand for nonlinear control, e.g. flatness-based control (Fliess et al., 1995), (Aschemann and Hofer, 2004). For the practical investigation of control approaches the test rig shown in figure 1 has been built. Two guideways with roller bearing units allow for rectilinear movements of a carriage with small nonlinear friction forces. On opposite sides of the carriage, pneumatic muscles are arranged in an antagonistic configuration between the carriage and the rigid frame. The mass flow of air of each pneumatic muscle is controlled by means of a proportional valve. The in-flowing air is provided at a maximum pressure of 7 bar, whereas the out-flowing air is discharged at atmospheric pressure, i.e. 1 bar. Pressure declines in the case of large commanded mass flows are counteracted by using compensator reservoirs, which maintain an approximately constant pressure supply level for each pneumatic muscle. Similarly, an additional compensator reservoir in combination with a sound absorber reduces the noise caused by discharged air. The paper is structured as follows: first, the modelling of the mechatronic system is addressed. Second, a nonlinear cascade control scheme is proposed: nonlinear H_2-optimal control loops, which can be realised with high bandwidth, guarantee a specified internal pressure in each pneumatic muscle (Aschemann et al., 2006). The outer control loop involves nonlinear model predictive trajectory control of the carriage position and the mean muscle pressure as controlled variables and provides the reference pressures for the inner pressure control loops. Aiming at good tracking behaviour, feedforward control based on differential flatness is considered in the control structure as well. A disturbance force resulting from remaining modelling errors w.r.t. the force characteristic of the pneumatic

Aschemann H. and Schindele D. (2007).
NONLINEAR MODEL PREDICTIVE CONTROL OF A LINEAR AXIS BASED ON PNEUMATIC MUSCLES.
In *Proceedings of the Fourth International Conference on Informatics in Control, Automation and Robotics*, pages 92-99
DOI: 10.5220/0001649200920099

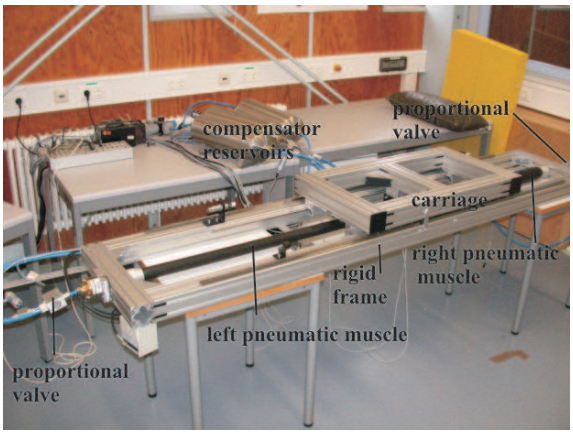

Figure 1: Linear axis test rig.

muscles as well as the friction characteristic of the carriage is estimated by a reduced-order disturbance observer and used for compensation in the nonlinear control scheme. By this, desired trajectories for both carriage position and mean pressure can be tracked with high accuracy as shown by experimental results from an implementation at the test rig.

2 SYSTEM MODELLING

As for modelling, the mechatronic system is divided in a pneumatic subsystem and a mechanical subsystem, which are coupled by the tension forces of the two pneumatic muscles. In contrast to the model of (Carbonell et al., 2001) the dynamics of the pneumatic subsystem is also included. The tension force $F_{Mi} \geq 0$ and the volume V_{Mi} of the pneumatic muscle i, $i = r, l$, nonlinearly depend on the according internal pressure p_{Mi} as well as the contraction length $\Delta\ell_{Mi}$. The origin of the generalised coordinate $x_S(t)$ of the carriage is defined as the position where the right muscle is fully contracted. Then, the constraints

$$\Delta\ell_{Ml}(x_S) = x_S, \;\; \Delta\ell_{Mr}(x_S) = \Delta\ell_{M,\max} - x_S \tag{1}$$

hold. Consequently, the contraction lengths of both pneumatic muscles are related to the carriage position.

2.1 Modelling of the Pneumatic Subsystem

The dynamics of the internal muscle pressure follows directly from a mass flow balance in combination with the energy equation for the compressed air in the muscle. As the internal muscle pressure is limited by a maximum value of $p_{Mi,max} = 7\ bar$, the ideal gas equation represents an accurate description of the thermodynamic behaviour. The thermodynamic process is modelled as a polytropic change of state with $n = 1.26$ as identified polytropic exponent. The identified volume characteristic of the pneumatic muscle can be described by a polynomial function

$$V_{Mi}\left(\Delta\ell_{Mi}, p_{Mi}\right) = \sum_{j=0}^{3} a_j \cdot \Delta\ell_{Mi}^{j} \cdot \sum_{k=0}^{1} b_k \cdot p_{Mi}^{k}. \tag{2}$$

with the contraction length $\Delta\ell_{Mi}$ and the muscle pressure p_{Mi}. The resulting state equation for the internal muscle pressure in the muscle i is given by

$$\dot{p}_{Mi} = \frac{n}{V_{Mi} + n \cdot \frac{\partial V_{Mi}}{\partial p_{Mi}} \cdot p_{Mi}} \left[R_L \cdot \vartheta(\cdot) \cdot \dot{m}_{Mi} - \frac{\partial V_{Mi}}{\partial \Delta\ell_{Mi}} \cdot \frac{\partial \Delta\ell_{Mi}}{\partial x_S} \cdot p_{Mi} \cdot \dot{x}_S\right], \tag{3}$$

where R_L denotes the gas constant of air. The function $\vartheta(n, T_S, T_{Mi}, sign(\dot{m}_{Mi}))$, which depends on the polytropic exponent n, the air supply temperature T_S, the internal temperature T_{Mi}, and the sign of the mass flow rate $\dot{m}_{Mi}$, can be approximated with good accuracy by the constant temperature T_0 of the ambiance. Thereby, temperature measurements can be avoided, and the implementational effort is significantly reduced.

2.2 Modelling of the Mechanical Subsystem

The mechanical subsystem is related to the motion of the carriage with mass $m_S = 30\ kg$ on its guideways. The nonlinear force characteristic $F_{Mi}(p_{Mi}, \Delta\ell_{Mi})$ of a pneumatic muscle represents the resulting tension force for given internal pressure p_{Mi} as well as given contraction length $\Delta\ell_{Mi}$. It has been identified by static measurements and, then, approximated by a polynomial description

$$F_{Mi}(\Delta\ell_{Mi}, p_{Mi}) = \bar{F}_{Mi}(\Delta\ell_{Mi}) \cdot p_{Mi} - f_{Mi}(\Delta\ell_{Mi}). \tag{4}$$

The equation of motion follows directly from Newton's second law as a second order differential equation for the carriage position

$$m_S \cdot \ddot{x}_S = F_{Ml}\left(\cdot\right) - F_{Mr}\left(\cdot\right) - F_U. \tag{5}$$

At this, remaining model uncertainties are taken into account by the disturbance force F_U. These uncertainties stem from approximation errors concerning the static muscle force characteristics, non-modelled viscoelastic effects of the vulcanised rubber material, and viscous damping as well as friction forces acting on the carriage.

3 NORM-OPTIMAL CONTROL OF THE MUSCLE PRESSURES

In the sequel, the nonlinear norm-optimal control design is presented (Lukes, 1969). The design approach applies to the following class of systems

$$\begin{aligned}\dot{\boldsymbol{x}}(t) &= \boldsymbol{A}\boldsymbol{x}(t) + \boldsymbol{B}\boldsymbol{u}(t) + \boldsymbol{f}\left(\boldsymbol{x}(t), \boldsymbol{u}(t)\right), \\ \boldsymbol{y} &= \boldsymbol{h}\left(\boldsymbol{x}(t), \boldsymbol{u}(t)\right) = \boldsymbol{C}\boldsymbol{x}(t) + \boldsymbol{D}\boldsymbol{u}(t),\end{aligned} \tag{6}$$

with the affine control input $\boldsymbol{u} \in \mathcal{U} \subset \mathbb{R}^m$, the state vector $\boldsymbol{x} \in \mathcal{X} \subset \mathbb{R}^n$ and the output vector $\boldsymbol{y} \in \mathcal{Y} \subset \mathbb{R}^p$. The non-linearity $\boldsymbol{f}(\boldsymbol{x}, \boldsymbol{u})$ can be stated as $\boldsymbol{f}(\boldsymbol{x}, \boldsymbol{u}) = \boldsymbol{f}^{(2)}(\boldsymbol{x}, \boldsymbol{u}) + \boldsymbol{f}^{(3)}(\boldsymbol{x}, \boldsymbol{u}) + ...$, where $\boldsymbol{f}^{(m)}(\boldsymbol{x}, \boldsymbol{u})$ denotes a polynomial of degree m in terms of $\boldsymbol{x}$ and $\boldsymbol{u}$. The H_2-optimal control aims at calculating a nonlinear state feedback law $\boldsymbol{u}(\boldsymbol{x})$ with $\boldsymbol{u}(\boldsymbol{0}) = \boldsymbol{0}$ such that the nonlinear cost function

$$J(\boldsymbol{u}) = \inf_{\boldsymbol{u} \in L_2^m[0,\infty)} \int_0^\infty \Lambda_2(\boldsymbol{x}, \boldsymbol{u}) \mathrm{d}t \tag{7}$$

with

$$\begin{aligned}\Lambda_2(\boldsymbol{x}, \boldsymbol{u}) =& \frac{1}{2}\left(\boldsymbol{y}^T\boldsymbol{Q}\boldsymbol{y} + \boldsymbol{u}^T\boldsymbol{R}\boldsymbol{u}\right) + l(\boldsymbol{x}, \boldsymbol{u}) \\ =& \frac{1}{2}\boldsymbol{x}^T\tilde{\boldsymbol{Q}}\boldsymbol{x} + \frac{1}{2}\boldsymbol{u}^T\tilde{\boldsymbol{R}}\boldsymbol{u} + \boldsymbol{x}^T\boldsymbol{N}\boldsymbol{u} + l(\boldsymbol{x}, \boldsymbol{u})\end{aligned} \tag{8}$$

is minimized. The symmetric, positive definite weighting matrix $\boldsymbol{Q} = \boldsymbol{Q}^T > 0$ accounts for the output variables, whereas the symmetric, positive definite weighting matrix $\boldsymbol{R}$ regards the control inputs. The nonlinear term $l(\boldsymbol{x}, \boldsymbol{u}) = l^{(3)}(\boldsymbol{x}, \boldsymbol{u}) + l^{(4)}(\boldsymbol{x}, \boldsymbol{u}) + ...$ consists of expressions of third or higher degrees in terms of $\boldsymbol{x}$ and $\boldsymbol{u}$. In the case of $l(\boldsymbol{x}, \boldsymbol{u}) = 0$ the cost function becomes quadratic. The solution of the above stated optimization problem is given by the positive definite solution $\mathcal{J}(\boldsymbol{x}) : \mathcal{X} \rightarrow \mathbb{R}^+$ of a nonlinear partial differential equation, the Hamilton-Jacobi-Bellman-equation (HJB-equation)

$$\min_{\boldsymbol{u}} H\left(\boldsymbol{x}, \mathcal{J}_x(\boldsymbol{x}), \boldsymbol{u}\right) = 0, \tag{9}$$

with the corresponding Hamiltonian

$$H = \mathcal{J}_x(\boldsymbol{x})\left[\boldsymbol{A}\boldsymbol{x} + \boldsymbol{B}\boldsymbol{u} + \boldsymbol{f}(\boldsymbol{x}, \boldsymbol{u})\right] + \Lambda_2(\boldsymbol{x}, \boldsymbol{u}). \tag{10}$$

In the considered unconstrained case, the optimal solution $\boldsymbol{u}^*$ is obtained from the stationary condition $H_u = 0$. Consequently, the two equations

$$\begin{aligned}H =& \mathcal{J}_x(\boldsymbol{x})\left[\boldsymbol{A}\boldsymbol{x} + \boldsymbol{B}\boldsymbol{u} + \boldsymbol{f}(\boldsymbol{x}, \boldsymbol{u})\right] + \frac{1}{2}\boldsymbol{x}^T\tilde{\boldsymbol{Q}}\boldsymbol{x} \\ &+ \boldsymbol{x}^T\boldsymbol{N}\boldsymbol{u} + \frac{1}{2}\boldsymbol{u}^T\tilde{\boldsymbol{R}}\boldsymbol{u} + l(\boldsymbol{x}, \boldsymbol{u}) = 0\end{aligned} \tag{11}$$

and

$$\begin{aligned}H_u =& \mathcal{J}_x(\boldsymbol{x})\left(\boldsymbol{B} + \boldsymbol{f}_u(\boldsymbol{x}, \boldsymbol{u})\right) + \boldsymbol{x}^T\boldsymbol{N} \\ &+ \boldsymbol{u}^T\tilde{\boldsymbol{R}} + l_u(\boldsymbol{x}, \boldsymbol{u}) = 0\end{aligned} \tag{12}$$

need to be solved. These equations are approximately solved by an approach according to (Lukes, 1969) based on power series expansions of the involved nonlinear functions . The gradient of the optimal solution $\mathcal{J}(\boldsymbol{x})$ and the control law are recursively determined by a step-by-step solution of both equations for a considered degree k of the according polynomials in $\boldsymbol{x}$ and $\boldsymbol{u}$.

3.1 Feedback Control Design

The control design for both internal muscle pressures is identical (Aschemann et al., 2006). For the sake of simplicity, the internal muscle pressure as state variable is denoted as $x := p_{Mi}$, $i = \{r, l\}$, and the control input as $u := u_{pi} = R_L \cdot T_0 \cdot \dot{m}_{Mi}$. Then, the state equation (3) can be rewritten as

$$\dot{x} = \frac{n \cdot \left(u - k_1(x_S, \dot{x}_S) \cdot x - k_2(x_S, \dot{x}_S) \cdot x^2\right)}{k_3(x_S) + k_4(x_S) \cdot x}, \tag{13}$$

According to the continuous dependence of the coefficients $k_i(x_S, \dot{x}_S)$ on x_S and $\dot{x}_S$, the resulting feedback control law is adapted by gain-scheduling. After a truncated Taylor series expansion with respect to $x = p_{Mi}$, the nonlinear state space description for the muscles pressure becomes

$$\begin{aligned}\dot{x} &= a(u) + b(u) \cdot x + c(u) \cdot x^2 + d(u) \cdot x^3 \\ &\quad + e(u) \cdot x^4 + g(u) \cdot x^5, \\ y &= x,\end{aligned} \tag{14}$$

The quadratic cost function with $l(x, u) = 0$ is given by

$$J(u) = \frac{1}{2}\int_0^\infty \left(q_p x^2 + r_p u^2\right) \mathrm{d}t, \tag{15}$$

where the scalar r_p serves as a weighting factor for the input variable $u = u_{pi}$ and the scalar q_p as weighting factor for the state variable, i.e. the muscle pressure $x = p_{Mi}$. The H_2-optimal control laws for these fast inner control loops are calculated up to the degree $k = 3$, i.e. $u_{pi,FB}(x) = \sum_{j=1}^{3} u^{0(j)}$. The resulting nonlinear feedback control law $u_{pl,FB}(p_{Ml}, x_S, \dot{x}_S)$ for the left muscle is depicted in Fig. 2 for $\dot{x}_S = 0.1$ m/s. Obviously, the linear part dominates the nonlinear terms.

3.2 Feedforward Control Design

As for feedforward control design, differential flatness can be exploited for the system under consideration (Fliess et al., 1995). The muscle pressure

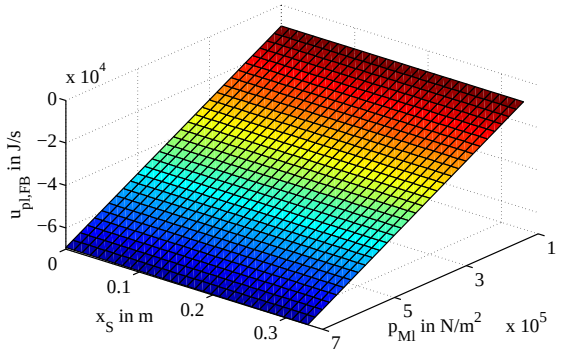

Figure 2: Nonlinear H_2-optimal feedback control law $u_{pl,FB}(p_{Ml}, x_S, \dot{x}_S)$ for the left pneumatic muscle for the gain-scheduling parameters x_S and $\dot{x}_S = 0.1$ m/s.

$y = p_{Mi}$, $i = \{r, l\}$, obviously represents a flat output of the corresponding inner control loop. Evaluating the state equation (3) for the muscle pressure with desired values for the flat output $y_d = p_{Mid}$ as well as its time derivative $\dot{y}_p = \dot{p}_{Mid}$ and solving for the feedforward control part $u_{pi,FF}$ result in

$$u_{pi,FF} = \left(\frac{V_{Mi}}{n} + \frac{\partial V_{Mi}}{\partial p_{Mi}} \cdot p_{Mid}\right) \dot{p}_{Mid} + \frac{\partial V_{Mi}}{\partial \Delta l_{Mi}} \frac{\partial \Delta l_{Mi}}{\partial x_S} \cdot \dot{x}_S \cdot p_{Mid} - u_{pi,FB}(p_{Mid}). \tag{16}$$

Note that the measured values x_S and $\dot{x}_S$ are used for a gain-scheduled adaptation of the feedforward control law. As a result, the overall control law for the inner control loops becomes $u_{pi} = u_{pi,FF} + u_{pi,FB}$.

4 NONLINEAR MPC

The main idea of the control approach consists in a minimization of a future tracking error in terms of the predicted state vector based on the actual state and the desired state vector resulting from trajectory planning (Lizarralde et al., 1999), (Jung and Wen, 2004). The minimization is achieved by repeated approximate numerical optimization in each time step, in the given case using the Newton-Raphson technique. The optimization is initialised in each time step with the optimization result of the preceeding time step in form of the input vector. The NMPC-algorithm is based on the following nonlinear discrete-time state space representation

$$\boldsymbol{x}_{k+1} = \boldsymbol{f}(\boldsymbol{x}_k, \boldsymbol{u}_k)\ ,\ \boldsymbol{y}_k = \boldsymbol{h}(\boldsymbol{x}_k, \boldsymbol{u}_k)\ , \tag{17}$$

with the state vector $\boldsymbol{x}_k \in \mathbb{R}^n$, the control input $\boldsymbol{u}_k \in \mathbb{R}^m$ and the output vector $\boldsymbol{y}_k \in \mathbb{R}^p$. The constant M specifies the prediction horizon T_P as a multiple of the sampling time t_s, i.e. $T_P = M \cdot t_s$. The predicted input vector at time k becomes

$$\boldsymbol{u}_{k,M} = \left[{\boldsymbol{u}_1^{(k)}}^T, ..., {\boldsymbol{u}_M^{(k)}}^T\right]^T\ , \tag{18}$$

with $\boldsymbol{u}_{k,M} \in \mathbb{R}^{m \cdot M}$. The predicted state vector at the end of the prediction horizon $\boldsymbol{\phi}_M(\boldsymbol{x}_k, \boldsymbol{u}_{k,M})$ is obtained by repeated substitution of k by $k+1$ in the discrete-time state equation (17)

$$\begin{aligned} \boldsymbol{x}_{k+2} &= \boldsymbol{f}(\boldsymbol{x}_{k+1}, \boldsymbol{u}_{k+1}) = \boldsymbol{f}(\boldsymbol{f}(\boldsymbol{x}_k, \boldsymbol{u}_k), \boldsymbol{u}_{k+1}) \\ &\vdots \\ \boldsymbol{x}_{k+M} &= \underbrace{\boldsymbol{f}(\cdots \boldsymbol{f}}_{M}(\boldsymbol{x}_k, \underbrace{\boldsymbol{u}_k), \cdots, \boldsymbol{u}_{k+M-1}}_{M}) \\ &= \boldsymbol{\phi}_M(\boldsymbol{x}_k, \boldsymbol{u}_{k,M})\ . \end{aligned} \tag{19}$$

The difference of $\boldsymbol{\phi}_M(\boldsymbol{x}_k, \boldsymbol{u}_{k,M})$ and the desired state vector $\boldsymbol{x}_d$ leads to the final control error

$$\boldsymbol{e}_{M,k} = \boldsymbol{\phi}_M(\boldsymbol{x}_k, \boldsymbol{u}_{k,M}) - \boldsymbol{x}_d\ , \tag{20}$$

i.e. to the control error at the end of the prediction horizon. The cost function to be minimized follows as

$$J_{MPC} = \frac{1}{2} \cdot \boldsymbol{e}_{M,k}^T \boldsymbol{e}_{M,k}\ , \tag{21}$$

and, hence, the necessary condition for an extremum can be stated as

$$\frac{\partial J_{MPC}}{\partial \boldsymbol{e}_{M,k}} = \boldsymbol{e}_{M,k} \stackrel{!}{=} 0\ . \tag{22}$$

A Taylor-series expansion of (22) at $\boldsymbol{u}_{k,M}$ in the neighbourhood of the optimal solution leads to the following system of equations

$$\boldsymbol{0} = \boldsymbol{e}_{M,k} + \frac{\partial \boldsymbol{\phi}_M}{\partial \boldsymbol{u}_{k,M}} \Delta \boldsymbol{u}_{k,M} + T.h.O. \tag{23}$$

The vector $\Delta \boldsymbol{u}_{k,M}$ denotes the difference which has to be added to the input vector $\boldsymbol{u}_{k,M}$ to obtain the optimal solution. The n equations (23) represent an under-determined set of equations with $m \cdot M$ unknowns having an infinite number of solutions. A unique solution for $\Delta \boldsymbol{u}_{k,M}$ can be determined by solving the following L_2-optimization problem with (23) as side condition

$$J = \frac{1}{2} \cdot \Delta \boldsymbol{u}_{k,M}^T \Delta \boldsymbol{u}_{k,M} + \boldsymbol{\lambda}^T \left(\boldsymbol{e}_{M,k} + \frac{\partial \boldsymbol{\phi}_M}{\partial \boldsymbol{u}_{k,M}} \Delta \boldsymbol{u}_{k,M}\right)\ . \tag{24}$$

Consequently, the necessary conditions can be stated as

$$\begin{aligned} \frac{\partial J}{\partial \Delta \boldsymbol{u}_{k,M}} \stackrel{!}{=} 0 &= \Delta \boldsymbol{u}_{k,M} + \left(\frac{\partial \boldsymbol{\phi}_M}{\partial \boldsymbol{u}_{k,M}}\right)^T \boldsymbol{\lambda}, \\ \frac{\partial J}{\partial \boldsymbol{\lambda}} \stackrel{!}{=} 0 &= \boldsymbol{e}_{M,k} + \frac{\partial \boldsymbol{\phi}_M}{\partial \boldsymbol{u}_{k,M}} \Delta \boldsymbol{u}_{k,M}, \end{aligned} \tag{25}$$

which leads to $\boldsymbol{e}_{M,k}$:

$$\boldsymbol{e}_{M,k} = \underbrace{\frac{\partial \boldsymbol{\phi}_M}{\partial \boldsymbol{u}_{k,M}} \left(\frac{\partial \boldsymbol{\phi}_M}{\boldsymbol{u}_{k,M}} \right)^T}_{\boldsymbol{S}(\boldsymbol{\phi}_M, \boldsymbol{u}_{k,M})} \boldsymbol{\lambda} \,. \tag{26}$$

If the matrix $\boldsymbol{S}\left(\boldsymbol{\phi}_M, \boldsymbol{u}_{k,M}\right)$ is invertible, the vector $\boldsymbol{\lambda}$ can be calculated

$$\boldsymbol{\lambda} = \boldsymbol{S}^{-1}\left(\boldsymbol{\phi}_M, \boldsymbol{u}_{k,M}\right) \boldsymbol{e}_{M,k} \,. \tag{27}$$

An almost singular matrix $\boldsymbol{S}\left(\boldsymbol{\phi}_M, \boldsymbol{u}_{k,M}\right)$ can be treated by a modification of (27)

$$\boldsymbol{\lambda} = \left[\mu \boldsymbol{I} + \boldsymbol{S}\left(\boldsymbol{\phi}_M, \boldsymbol{u}_{k,M}\right)\right]^{-1} \boldsymbol{e}_{M,k} \,, \tag{28}$$

where $\boldsymbol{I}$ denotes the unity matrix. The regularisation parameter $\mu > 0$ in (28) may be chosen constant or may be calculated by a sophisticated algorithm. The latter solution improves the convergence of the optimization but increases, however, the computational complexity. Solving (25) for $\Delta \boldsymbol{u}_{k,M}$ and inserting $\boldsymbol{\lambda}$ according to (27) or (28), directly leads to the L_2-optimal solution

$$\begin{aligned} \Delta \boldsymbol{u}_{k,M} &= -\left(\frac{\partial \phi_M}{\partial \boldsymbol{u}_{k,M}} \right)^T \boldsymbol{S}^{-1}\left(\boldsymbol{\phi}_M, \boldsymbol{u}_{k,M}\right) \boldsymbol{e}_{M,k} \\ &= -\left(\frac{\partial \phi_M}{\partial \boldsymbol{u}_{k,M}} \right)^{\dagger} \boldsymbol{e}_{M,k} \,. \end{aligned} \tag{29}$$

Here, $\left(\frac{\partial \phi_M}{\partial \boldsymbol{u}_{k,M}}\right)^{\dagger}$ denotes the Moore-Penrose pseudo inverse of $\frac{\partial \phi_M}{\partial \boldsymbol{u}_{k,M}}$. The overall NMPC-algorithm can be described as follows:
Choice of the initial input vector $\boldsymbol{u}_{0,M}$ at time $k = 0$, e.g. $\boldsymbol{u}_{0,M} = \boldsymbol{0}$, and repetition of steps a) - c) at each sampling time $k \geq 0$:

a) Calculation of an improved input vector $\boldsymbol{v}_{k,M}$ according to

$$\boldsymbol{v}_{k,M} = \boldsymbol{u}_{k,M} - \eta_k \left(\frac{\partial \boldsymbol{\phi}_M}{\partial \boldsymbol{u}_{k,M}} \right)^{\dagger} \boldsymbol{e}_{M,k} \,. \tag{30}$$

The step width η_k can be determined with, e.g., the Armijo-rule.

b) For the calculation of $\boldsymbol{u}_{k+1,M}$ the elements of the vector $\boldsymbol{v}_{k,M}$ have to be shifted by m elements and the steady-state input vector $\boldsymbol{u}_d$ corresponding to the final state has to be inserted at the end $\boldsymbol{u}_d$

$$\begin{aligned} \boldsymbol{u}_{k+1,M} = &\begin{bmatrix} \boldsymbol{0}_{(m(M-1)\times m)} \\ \boldsymbol{I}_{(m)} \end{bmatrix} \boldsymbol{u}_d \\ &+ \begin{bmatrix} \boldsymbol{0}_{(m(M-1)\times m)} & \boldsymbol{I}_{(m(M-1))} \\ \boldsymbol{0}_{m\times m} & \boldsymbol{0}_{(m\times m(M-1))} \end{bmatrix} \boldsymbol{v}_{k,M}. \end{aligned} \tag{31}$$

In general, the steady-state control input $\boldsymbol{u}_d$ can be computed from

$$\boldsymbol{x}_d = \boldsymbol{f}(\boldsymbol{x}_d, \boldsymbol{u}_d). \tag{32}$$

For differentially flat systems the desired input vector $\boldsymbol{u}_d$ is given by the inverse dynamics and can be stated as a function of the flat outputs and their time derivatives.

c) The first m elements of the improved input vector $\boldsymbol{v}_{k,M}$ are applied as control input at time k

$$\boldsymbol{u}_k = \begin{bmatrix} \boldsymbol{I}_{(m)} & \boldsymbol{0}_{(m\times m(M-1))} \end{bmatrix} \boldsymbol{v}_{k,M} \,. \tag{33}$$

In the proposed algorithm only one iteration is performed per time step. A similar approach using several iteration steps is described in (Weidemann et al., 2004).

4.1 Numerical Calculations

The analytical computation of the Jacobian $\frac{\partial \phi_M}{\partial \boldsymbol{u}_{k,M}}$ becomes increasingly complex for larger values of M. Therefore, a numerical approach is preferred taking advantage of the chain rule with $i = 0, ..., M-1$

$$\begin{aligned} \frac{\partial \phi_M}{\partial \mathbf{u}_{i+1}^{(k)}} = &\frac{\partial \phi_M}{\partial \mathbf{x}_{k+M-1}} \cdot \frac{\partial \mathbf{x}_{k+M-1}}{\partial \mathbf{x}_{k+M-2}} \cdot \ldots \\ &\cdot \frac{\partial \mathbf{x}_{k+i+2}}{\partial \mathbf{x}_{k+i+1}} \cdot \frac{\partial \mathbf{x}_{k+i+1}}{\partial \mathbf{u}_{i+1}^{(k)}} \,. \end{aligned} \tag{34}$$

Introducing the abbreviations

$$\boldsymbol{A}_i := \frac{\partial \boldsymbol{x}_{k+i+1}}{\partial \boldsymbol{x}_{k+i}} = \frac{\partial \boldsymbol{f}}{\partial \boldsymbol{x}} \left(\boldsymbol{x}_{k+i}, \boldsymbol{u}_{i+1}^{(k)} \right) \,, \tag{35}$$

$$\boldsymbol{B}_i := \frac{\partial \boldsymbol{x}_{k+i+1}}{\partial \boldsymbol{u}_{i+1}^{(k)}} = \frac{\partial \boldsymbol{f}}{\partial \boldsymbol{u}} \left(\boldsymbol{x}_{k+i}, \boldsymbol{u}_{i+1}^{(k)} \right) \,, \tag{36}$$

the Jacobian can be computed as follows

$$\begin{aligned} \frac{\partial \phi_M}{\partial \mathbf{u}_{k,M}} = &[\mathbf{A}_{M-1}\mathbf{A}_{M-2}\cdots\mathbf{A}_1\mathbf{B}_0, \\ &\mathbf{A}_{M-1}\cdots\mathbf{A}_2\mathbf{B}_1, ..., \mathbf{A}_{M-1}\mathbf{B}_{M-2}, \mathbf{B}_{M-1}] \,. \end{aligned} \tag{37}$$

For the inversion of the symmetric and positive definite matrix $\boldsymbol{S}\left(\boldsymbol{\phi}_M, \boldsymbol{u}_{k,M}\right) = \frac{\partial \boldsymbol{\phi}_M}{\partial \boldsymbol{u}_{k,M}} \left(\frac{\partial \boldsymbol{\phi}_M}{\partial \boldsymbol{u}_{k,M}} \right)^T$ the Cholesky-decomposition has proved advantageous in terms of computational effort.

4.2 Choice of the Nmpc Design Parameters

The most important NMPC design parameter is the prediction horizon T_P, which is given as the product of the sampling time t_s and the constant value

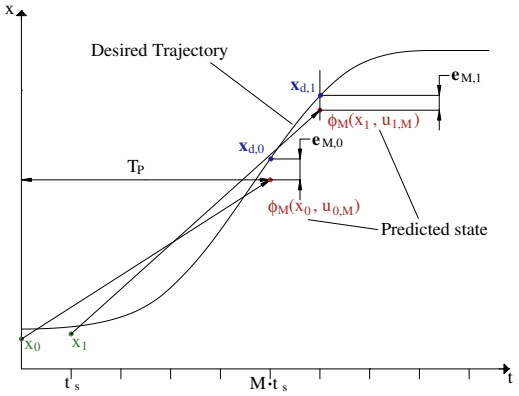

Figure 3: Design parameters.

M. Large values of T_P lead to a slow and smooth transient behaviour and result in a robust and stable control loop. For fast trajectory tracking, however, a smaller value T_P is desirable concerning a small tracking error. The choice of the sampling time t_s is crucial as well: a small sampling time is necessary regarding discretization error and stability; however, the NMPC-algorithm has to be evaluated in real-time within the sampling inverval. Furthermore, the smaller t_s, the larger becomes M for a given prediction horizon, which in turn increases the computational complexity of the optimization step. Consequently, a system-specific trade-off has to be made for the choice of M and t_s. This paper follows the moving horizon approach with a constant prediction horizon and, hence, a constant dimension $m \cdot M$ of the corresponding optimization problem in constrast to the shrinking horizon approach (Weidemann et al., 2004).

4.3 Input Constraints

One major advantage of predictive control is the possibility to easily account for input constraints, which are present in almost all control applications. To this end, the cost function can be extended with a corresponding term

$$h(\boldsymbol{u}_j^{(k)}) = \begin{cases} 0 & \boldsymbol{u}_{min} \leq \boldsymbol{u}_j^{(k)} \leq \boldsymbol{u}_{max} \\ g_1(\boldsymbol{u}_j^{(k)}) \text{ for } & \boldsymbol{u}_j^{(k)} > \boldsymbol{u}_{max} \\ g_2(\boldsymbol{u}_j^{(k)}) & \boldsymbol{u}_j^{(k)} < \boldsymbol{u}_{min} \end{cases} , \tag{38}$$

which has to be evaluated componentwise, i.e. for each input variable at each sampling time. Thus, the contribution of the additional input constraints depending on $\boldsymbol{u}_{k,M}$ is given by

$$z(\boldsymbol{u}_{k,M}) = \sum_{j=1}^{M} h(\boldsymbol{u}_j^{(k)}) \tag{39}$$

Instead of $\boldsymbol{e}_{M,k}$ the vector $\left[\boldsymbol{e}_{M,k}^T, z\right]^T$ has to be minimized in the NMPC-algorithm.

5 MODIFICATIONS OF THE ALGORITHM

To improve trajectory tracking behaviour, the NMPC-algorithm can be modified as follows:
(1) Instead of a minimization of the control error at the end of the prediction horizon given by the difference of the predicted value $\boldsymbol{\phi}_M(\boldsymbol{x}_k, \boldsymbol{u}_{k,M})$ and the according reference value $\boldsymbol{x}_d$, the minimization could take into account additional predicted errors $\boldsymbol{e}_{Mi,k} = \boldsymbol{\phi}_{Mi}(\boldsymbol{x}_k, \boldsymbol{u}_{k,Mi}) - \boldsymbol{x}_{di}$, $i \in \mathbb{N}$, $Mi < M$. Thus, the cost function (21) is modified as follows

$$J_{MPC} = \frac{1}{2}(\boldsymbol{e}_{M1,k}^T \boldsymbol{e}_{M1,k} + ... + \boldsymbol{e}_{M,k}^T \boldsymbol{e}_{M,k}) \tag{40}$$

The required values $\boldsymbol{\phi}_{Mi}$ are already known from the calculation of $\boldsymbol{\phi}_M$ and, hence, do not further increase the computational effort. Unfortunately, the additional computation of $\frac{\partial \boldsymbol{\phi}_{Mi}}{\partial \boldsymbol{u}_{Mi,k}}$ as well as the increased dimension of the matrix to be inverted $\boldsymbol{S}(\boldsymbol{\phi}_{M1}, ..., \boldsymbol{\phi}_M, \boldsymbol{u}_{k,M1}, ..., \boldsymbol{u}_{k,M})$ have a significant impact on the computation time. Therefore, the number of expressions in the cost function should be kept as small as possible, especially in the given case of a fast higher-dimensional system.
(2) A further improvement of the trajectory tracking behaviour can be achieved if an input vector resulting from an inverse system model is used as initial vector for the subsequent optimization step instead of the last input vector. Since the system under consideration is differentially flat (Aschemann and Hofer, 2004), the required ideal control input can be derived for a given reference trajectory. The slightly modified algorithm can be stated as follows

a) Calculation of the ideal input vector $\boldsymbol{u}_{k,M}^{(d)}$ by evaluating an inverse system model with the specified reference trajectory as well as a certain number $\beta \in \mathbb{N}$ of its time derivatives

$$\boldsymbol{u}_{k,M}^{(d)} = \boldsymbol{u}_{k,M}^{(d)} \left(\boldsymbol{y}_d, \dot{\boldsymbol{y}}_d, ..., \overset{(\beta)}{\boldsymbol{y}}_d \right) . \tag{41}$$

b) Calculation of the improved input vector $\boldsymbol{v}_{k,M}$ based on the equation

$$\boldsymbol{v}_{k,M} = \boldsymbol{u}_{k,M}^{(d)} - \eta_k \left(\frac{\partial \boldsymbol{\phi}_M}{\partial \boldsymbol{u}_{k,M}} \right)^{\dagger} \boldsymbol{e}_{M,k} . \tag{42}$$

c) Application of the first m elements of $\boldsymbol{v}_{k,M}$ to the process

$$\boldsymbol{u}_k = \left[\begin{array}{cc} \boldsymbol{I}_{(m)} & \boldsymbol{0}_{(m \times m(M-1))} \end{array} \right] \boldsymbol{v}_{k,M} \; . \quad (43)$$

If the reference trajectory is known in advance, the according reference input vector $\boldsymbol{u}_{k,M}^{(d)}$ can be computed offline. Consequently, the online computational time remains unaffected. Of course, all the proposed modifications could be combined.

5.1 Nmpc of the Carriage Position

The state space representation for the position control design can be directly derived from the equation of motion for the carriage

$$\dot{\boldsymbol{x}} = \left[\begin{array}{c} \dot{x}_S \\ \ddot{x}_S \end{array} \right] = \left[\begin{array}{c} \dot{x}_S \\ \frac{F_{Ml}(x_S, p_{Ml}) - F_{Mr}(x_S, p_{Mr})}{m_S} \end{array} \right] . \quad (44)$$

The carriage position x_S and the carriage velocity $\dot{x}_S$ represent the state variables, whereas the input vector consists of the left as well as the right internal muscle pressure, p_{Ml} and p_{Mr}. The discrete-time representation of the continous-time system (44) is obtained by Euler discretisation

$$\boldsymbol{x}_{k+1} = \boldsymbol{x}_k + t_s \cdot \boldsymbol{f}(\boldsymbol{x}_k, \boldsymbol{u}_k) \quad (45)$$

Using this simple discretisation method, the computational effort for the NMPC-algorithm can be kept acceptable. Furthermore, no significant improvement was obtained for the given system with the Heun discretisation method because of the small sampling time $t_s = 5 \; ms$. Only in the case of large sampling times, e.g. $t_s > 20 \; ms$, the increased computational effort caused by a sophisticated time discretisation method is advantageous. Then, the smaller discretisation error allows for less time integration steps for a specified prediction horizon, i.e. a smaller number M. As a result, the smaller number of time steps can overcompensate the larger effort necessary for a single time step. The flat output variables of (44) are given by

$$\boldsymbol{y} = \left[\begin{array}{c} x_S \\ p_M \end{array} \right] = \left[\begin{array}{c} x_S \\ \frac{1}{2} \cdot (p_{Ml} + p_{Mr}) \end{array} \right] . \quad (46)$$

Using the desired trajectories for the carriage position x_{Sd} and the mean muscle pressure p_{Md}, the corresponding desired input values result in

$$\boldsymbol{u}_d = \left[\begin{array}{c} p_{Mld} \\ p_{Mrd} \end{array} \right] = \frac{1}{\bar{F}_{Ml}(\cdot) + \bar{F}_{Mr}(\cdot)} \cdot \left[\begin{array}{c} f_{Ml}(\cdot) - f_{Mr}(\cdot) + 2\bar{F}_{Mr}(\cdot) p_{Md} + m_S \ddot{x}_{Sd} \\ f_{Mr}(\cdot) - f_{Ml}(\cdot) + 2\bar{F}_{Ml}(\cdot) p_{Md} - m_S \ddot{x}_{Sd} \end{array} \right] . \quad (47)$$

5.2 Compensation of the Valve Characteristic and Disturbances

The nonlinear valve characteristic (VC) is compensated by pre-multiplying with its inverse valve characteristic (IVC) in each input channel. Here, the inverse valve characteristic depends both on the commanded mass flow and on the measured internal pressure. Disturbance behaviour and tracking accuracy in view of model uncertainties can be significantly improved by introducing a compensating control action provided by a reduced-order disturbance observer, which uses an integrator as disturbance model. The observer design is based on the equation of motion for the carriage (5), where the variable F_U takes into account both the friction force F_{RS} and the remaining model uncertainties of the muscle force characteristics ΔF_M, i.e. $F_U = F_{RS} - \Delta F_M$. Moreover, the disturbance observer is capable of counteracting impacts of changing carriage mass Δm_S as well, which results in $F_U = F_{RS} + \Delta m_S \cdot \ddot{x}_S - \Delta F_M$. As the complete state vector $\mathbf{x} = [x_S, \dot{x}_S]^T$ is forthcoming, the reduced-order disturbance observer yields a disturbance force estimate $\hat{F}_U$. Disturbance compensation is achieved by using the estimated force $\hat{F}_U$ as additional control action after an appropriate input transformation.

6 EXPERIMENTAL RESULTS

For the experiments at the linear axis test rig the synchronized reference trajectories for the carriage position as well as the mean muscle pressure depicted in the upper part of fig. 4 have been used. First, several changes are specified for the carriage position between $0.02 \; m$ and $0.29 \; m$ at a constant mean pressure of $4 \; bar$. Second, the mean pressure is increased up to $5 \; bar$ and kept constant during some subsequent fast position variations by $-0.02 \; m$. Third, several larger position changes are performed with a constant mean pressure of $4 \; bar$.

During trajectory tracking the number M is set to small values. The sampling time has been kept constant at $t_s = 5 \; ms$. Fig. 4 shows the results obtained with the choice $M = 15, i.e. \; T_P = 75 \; ms$. Smaller prediction horizons would lead to a tendency towards increasing oscillatory behaviour and, finally, to instability. During the acceleration and deceleration intervalls a maximum position control error $e_{x,max}$ of approx. $4 \; mm$ occurs. The maximum control error of the mean pressure e_p is only slightly above an absolute value of approx. $0.12 \; bar$. The importance of

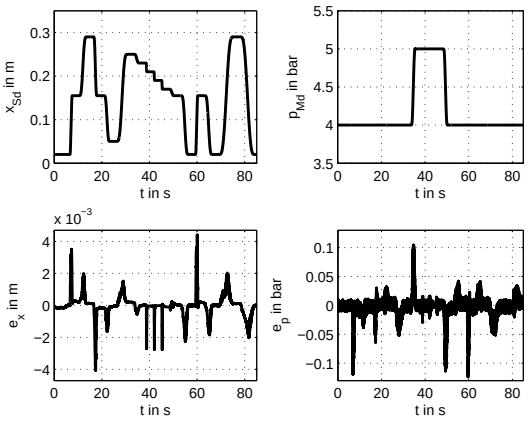

Figure 4: Reference trajectories and according tracking errors for carriage position and mean pressure ($T_P = 75\ ms$).

the observer-based disturbance compensation is emphasized by Fig. 5. Without this control part the maximum position control error increases up to approx. 7 mm.

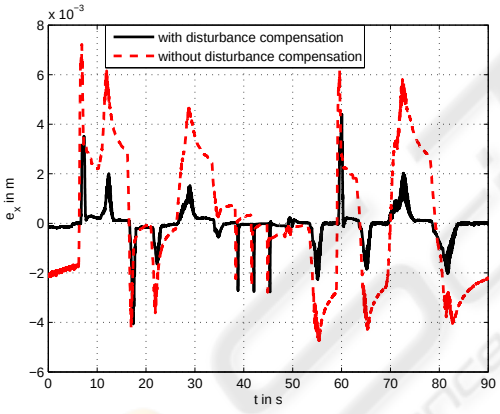

Figure 5: Position control error e_x with and without disturbance observer ($T_P = 75\ ms$).

7 CONCLUSIONS

In this paper, a cascaded trajectory control scheme using nonlinear optimal design is presented for a carriage driven by pneumatic muscles. The modelling of this mechatronic system leads to a system of four nonlinear differential equations. The nonlinear characteristics of the pneumatic muscles are approximated by polynomials. The nonlinearity of the valve is linearised by means of a pre-multiplication with its approximated inverse characteristic. The inner control loops of the cascade involve a norm-optimal control of the internal muscle pressure with high bandwidth. The outer nonlinear model predictive control loop is responsible for trajectory tracking with carriage position and mean pressure as controlled variables. Remaining model uncertainties are taken into account by a disturbance force estimated by means of a disturbance observer. Experimental results from an implementation on a test rig emphasise the excellent closed-loop performance with maximum position errors of $4\ mm$ during the movements, negligible steady-state position error and steady-state pressure error of less than $0.02\ bar$.

REFERENCES

Aschemann, H. and Hofer, E. (2004). Flatness-based trajectory control of a pneumatically driven carriage with model uncertainties. *Proceedings of NOLCOS 2004, Stuttgart, Germany*, pages 239 – 244.

Aschemann, H., Schindele, D., and Hofer, E. (2006). Nonlinear optimal control of a mechatronic system with pneumatic muscles actuators. *CD-ROM-Proceedings of MMAR 2006, Miedzyzdroje, Poland,*.

Carbonell, P., Jiang, Z. P., and Repperger, D. (2001). Comparative study of three nonlinear control strategies for a pneumatic muscle actuator. *Proceedings of NOLCOS 2001, Saint-Petersburg, Russia*, pages 167–172.

Fliess, M., Levine, J., Martin, P., and Rouchon, P. (1995). Flatness and defect of nonlinear systems: Introductory theory and examples. *Int. J. Control 61*, 6:1327 – 1361.

Jung, S. and Wen, J. (2004). Nonlinear model predictive control for the swing-up of a rotary inverted pendulum. *ASME J. of Dynamic Systems, Measurement and Control*, 126:666 – 673.

Lizarralde, F., Wen, J., and Hsu, L. (1999). A new model predictive control strategy for affine nonlinear control systems. *Proc of the American Control Conference (ACC '99), San Diego*, pages 4263 – 4267.

Lukes, D. (1969). Optimal regulation of nonlinear dynamical systems. *SIAM Journal Control*, 7:75 – 100.

Weidemann, D., Scherm, N., and Heimann, B. (2004). Discrete-time control by nonlinear online optimization on multiple shrinking horizons for underactuated manipulators. *Proceedings of the 15th CISM-IFToMM Symposium on Robot Design, Dynamics and Control, Montreal*.